Clim. Past Discuss., 10, 2547–2594, 2014
www.clim-past-discuss.net/10/2547/2014/
doi:10.5194/cpd-10-2547-2014

Climate of the Past
Discussions
Open Access

Interaction of ice sheets and climate during the past 800 000 years

L. B. Stap[1], R. S. W. van de Wal[1], B. de Boer[1,2], R. Bintanja[3], and L. J. Lourens[2]

[1]Institute for Marine and Atmospheric research Utrecht, Utrecht University, Princetonplein 5, 3584 CC Utrecht, the Netherlands
[2]Department of Earth Sciences, Faculty of Geosciences, Utrecht University, Budapestlaan 4, 3584 CD Utrecht, the Netherlands
[3]Royal Netherlands Meteorological Institute (KNMI), Wilhelminalaan 10, 3732 GK De Bilt, the Netherlands

Received: 22 May 2014 – Accepted: 2 June 2014 – Published: 23 June 2014

Correspondence to: L. B. Stap (l.b.stap@uu.nl)

Published by Copernicus Publications on behalf of the European Geosciences Union.

Abstract

During the Cenozoic, land ice and climate have interacted on many different time scales. On long time scales, the effect of land ice on global climate and sea level is mainly set by large ice sheets on North America, Eurasia, Greenland and Antarctica. The climatic forcing of these ice sheets is largely determined by the meridional temperature profile resulting from radiation and greenhouse gas (GHG) forcing. As response, the ice sheets cause an increase in albedo and surface elevation, which operates as a feedback in the climate system. To quantify the importance of these climate-land ice processes, a zonally-averaged energy balance climate model is coupled to five one-dimensional ice-sheet models, representing the major ice sheets.

In this study, we focus on the transient simulation of the past 800 000 years, where a high-confidence CO_2-record from ice cores samples is used as input in combination with Milankovitch radiation changes. We obtain simulations of atmospheric temperature, ice volume and sea level, that are in good agreement with recent proxy-data reconstructions. We examine long-term climate-ice sheet interactions by a comparison of simulations with uncoupled and coupled ice sheets. We show that these interactions amplify global temperature anomalies by up to a factor 2.6, and that they increase polar amplification by 94 %. We demonstrate that, on these long time scales, the ice-albedo feedback has a larger and more global influence on the meridional atmospheric temperature profile than the surface-height temperature feedback. Furthermore, we assess the influence of CO_2 and insolation, by performing runs with one or both of these variables held constant. We find that atmospheric temperature is controlled by a complex interaction of CO_2 and insolation, and both variables serve as thresholds for Northern Hemispheric glaciation.

1 Introduction

Earth's climate is characterised by glaciations and deglaciations of the Northern Hemisphere during the past 800 000 years. For this period, the Dome C ice core provides a record of CO_2, CH_4, N_2O and deuterium-based Antarctic temperature (EPICA community members, 2004; Loulergue et al., 2008; Spahni et al., 2005; Jouzel et al., 2007). The Antarctic atmospheric temperature is tightly connected to a reconstruction of sea level over the past five glacial cycles, based on Red Sea bulk sediment analysis (Rohling et al., 2009). Ice coring performed on the Greenland Ice Sheet indicate the local temperature variability (GRIP members, 1993; NGRIP members, 2004; Dahl-Jensen et al., 2013), extending back to the last interglacial. Greenland and Antarctic climate have been shown to correspond closely to each other (EPICA community members, 2006). Additionally, important information arises from deep-sea sediment records of benthic $\delta^{18}O$ (Zachos et al., 2008; Lisiecki and Raymo, 2005). These serve as an independent proxy for ice volume only after correction for the also contained deep-sea temperature signal. Köhler et al. (2010) combined data on the radiative forcing of solar insolation, greenhouse gases (GHGs) and model-deduced ice volume, sea ice, vegetation and dust, to identify the importance of these components in governing temperature variability. This hybrid model-data approach has given a comprehensive overview of the importance of the different factors that played a role in the past glacial-interglacial cycles. However, their inferred global cooling between present-day and the Last Glacial Maximum of 6.4–9.6 K was considerably larger than recent proxy-data reconstructed ones of 5.8 K (Schneider von Deimling et al., 2006), 3.0 K (Schmittner et al., 2011) and 4.0 K (Annan and Hargreaves, 2013). Model studies can help in understanding this mismatch, which is possibly explained by background climate-state dependency of water vapour, lapse rate and cloud feedback strengths (Köhler et al., 2010). In addition, climate models offer the possibility of assessing the importance of its components and the interaction between processes by comparing results with those obtained from runs

CPD
10, 2547–2594, 2014

with one or more variables kept constant. This can also provide insight in the processes governing polar amplification, the ratio of polar to global temperature change.

Modelling ice ages is a classical issue in climate dynamics. They cannot be simulated solely by solar variability, because of lacking power in the eccentricity (100 kyr) band. Likely, insolation forcing and internal climate feedbacks between climate, ice sheets, and terrestrial dust (Ganopolski and Calov, 2011) or the lithosphere-asthenosphere system (Abe-Ouchi et al., 2013) play a role. Several other studies stress the importance of CO_2 forcing as an important driver of climatic changes (e.g. Paillard and Parrenin, 2004). In addition, Ritz et al. (2011) showed the importance of ocean circulation using a coupled ocean–atmosphere model with ice sheet forcing. Still under debate is the precise role of long-term ice sheet-climate feedbacks in the climatic response to CO_2 and insolation forcing, which is the focus of this study.

Obviously, land ice and climate are intimately linked. When local temperature is cold enough, winter snow accumulation can exceed summer melt and as a result an ice sheet is formed. This ice sheet alters the climate in several ways. Two effects are most important on long time scales. Firstly, the ice sheet reflects more short-wave radiation than the underlying ground, leading to lower temperatures. This is known as the ice-albedo feedback. Secondly, the ice increases the height of the surface. The surface is then positioned higher in the atmosphere, where temperatures are lower. This is called the surface-height temperature feedback. The latter effect is partly counteracted by lowering of the ice sheet bed by the induced ice loading. The cooling, effectuated by the feedbacks, consequently leads to more ice formation. The coupled nature of land ice and climate calls for combined modelling.

Earlier modelling studies addressing long-term global ice volume variations used stand-alone ice-dynamical models (Bintanja et al., 2005; Bintanja and Van de Wal, 2008; De Boer et al., 2010, 2012). In these studies, the only information on climate consisted of globally uniform temperature perturbations with respect to PI climate. They obtained reconstructions of Northern Hemispheric temperature, ice volume, and sea level from benthic $\delta^{18}O$ data by an inverse routine. From that, a consistent CO_2 simulation was constructed based on a simple relation between the Northern Hemispheric temperature and CO_2 data from several proxy records (Van de Wal et al., 2011). These studies, however, lacked information on the meridional temperature distribution. Moreover, the representation of deep ocean temperatures was very simplistic and CO_2 was not incorporated in the model. Therefore, it was not possible to study the individual contributions of insolation, CO_2 and land ice on temperature and sea level.

In this study, we no longer use the inverse benthic δ^{18}O routine. Instead, we aim to quantify the influence of the aforementioned ice sheet-climate feedbacks, by coupling a climate model to a dynamical ice-sheet model. Several recent studies have used a similar approach, mostly using three-dimensional ice sheet/shelf models of a single ice sheet, asynchronously coupled to Earth-System Models of Intermediate Complexity (EMICs) or GCMs. In other cases, the ice sheet/shelf model is forced with look-up tables of climate, calculated beforehand by GCMs. These studies focused predominantly on relatively short timescales, e.g. the last glacial cycle (Helsen et al., 2013; Ganopolski et al., 2010) and the termination of the last interglacial (Herrington and Poulsen, 2011). Alternatively, they addressed a single climatic event, such as the Eocene-Oligocene boundary (DeConto and Pollard, 2003; Wilson et al., 2013), the Middle-Miocene Transition (Langebroek et al., 2009) or the possible future retreat of the Greenland Ice Sheet (Ridley et al., 2005). Transient runs at time scales spanning ~ 100 kyr (Abe-Ouchi et al., 2013; Ganopolski and Calov, 2011) to ~ Myr (Pollard et al., 2013) have also been performed, but to our knowledge no study simulated all the major ice sheets simultaneously in a fully coupled fashion. Here, we combine a Zonally averaged Energy Balance Climate Model (ZEBCM, Bintanja, 1997) and a one-dimensional Ice Sheet Model (ISM, De Boer et al., 2010). The relative simplicity and consequent short computation time of these models enable us to perform a large suite of model tests and 800 kyr-long transient simulations of global climate for all five major ice sheets. Furthermore, this set-up allows us to study different feedback mechanisms.

From the results of the coupled model, we obtain a reconstruction of ice volume, sea level and meridional temperature, driven by CO_2 and insolation. Firstly, we will present this reconstruction, along with sensitivity tests to various aspects of the coupled model and a comparison with existing data from proxies and models. Secondly, we will compare simulations with uncoupled and coupled ice sheets to assess the influence of climate-ice sheet feedbacks. By only passing ice extent or ice height to the climate model, we will differentiate between the effects of the ice-albedo feedback and the surface-height temperature feedback. Moreover, we will address polar amplification and climate sensitivity over these 800 kyr. Finally, the relative contributions of insolation and CO_2 to climate variability will be studied, by performing model runs with one of these variables held constant.

2 Models and methods

2.1 Zonally Averaged Energy Balance Climate Model

The Zonally Averaged Energy Balance Climate Model (ZEBCM) used in this study, is described in detail by Bintanja (1997). Briefly, it consists of a coupled atmosphere model, ocean model and sea-ice model, all zonally averaged. It is based on the model of North (1975). The atmosphere model has a latitudinal resolution of 5° and one layer in the vertical. It has a time step of 0.5 day and includes a radiative transfer scheme, describing radiative forcing by insolation, CO_2, and cloud cover and optical depth (Bintanja, 1996). Turbulent heat transport and divergence of meridional energy transport are parameterised. No hydrological scheme is included. The land cover is subdivided into a forest, grassland and permanent land ice fraction, and affects only the surface albedo. Snow cover on each surface type is calculated as a function of temperature. The ocean model has the same latitudinal resolution and consists of six layers in the vertical. It describes the zonally-averaged thermohaline circulation, with water flowing poleward in the upper layer and equatorward in the lowest layer. Upwelling takes place in the entire ocean basin, except in the two latitudinal boxes closest to the pole, where the water sinks. The sea-ice model, with a resolution of 1.25° is purely thermodynamical. Where the sea surface temperature drops below the freezing temperature of 35 PSU saline water (271.22 K), the ocean becomes (partially) covered with sea ice of a specified thickness. Similar to the vegetation, the sea ice is subject to snow cover.

In an earlier study, the model was used to study present-day (PD) and Last Glacial Maximum (LGM) climate (Bintanja and Oerlemans, 1996). In order to perform transient simulations, now we use insolation and CO_2 as time-dependent input variables. Monthly mean insolation follows from Laskar et al. (2004), averaged to 5° resolution and updated every 1000 years. The EPICA record (Jouzel et al., 2007), interpolated to yearly values, is used as CO_2 input. Cloud cover and optical depth remain at PD value throughout the run. The climate sensitivity of the original model was 1.9 °C per CO_2-doubling (Bintanja, 1997), on the lower end of the 1.5–4.5 °C range reported in IPCC-AR5 (IPCC, 2013). In this study, a higher sensitivity of 2.2 °C is established by two alterations: the radiative forcing induced by a doubling of CO_2 is increased from 3.5 to 3.7 $\mathrm{W\,m^{-2}}$, in agreement with Myhre et al. (1998); an additional water-vapour feedback term of 1 $\mathrm{W\,m^{-2}\,K^{-1}}$ is included in the parameterisation of clear-sky upgoing longwave radiation, based on Ritz et al. (2011). To account for non-CO_2 greenhouse gases, the radiative forcing of CO_2 is multiplied by a factor of 1.3. This is based on the mean enhancement of radiative forcing by CH_4 and N_2O over the last 800 kyr derived from proxy data, as analysed by Köhler et al. (2010). As in Bintanja (1995), the strength of the thermohaline circulation (C) is made a function of the surface water density difference ($\Delta\rho$) between the equatorial and polar (60–80° N and 50–70° S) waters:

$$\frac{C}{C_0} = 1 + \zeta\left(\frac{\Delta\rho}{\Delta\rho_0} - 1\right), \tag{1}$$

where the subscript $_0$ denotes PI values and ζ is a strength-controlling scaling parameter, set to 8. The density difference consists of a temperature-gradient term and a pseudo-salinity term. The temperature gradient is calculated from the equation of state for 35 PSU saline water (Gill, 1982). The pseudo-salinity term represents the effect of polar-water freshening by meltwater, by multiplying the change in polar surface-

CPD
10, 2547–2594, 2014

Interaction of ice sheets and climate during the past 800 000 years

L. B. Stap et al.

water temperature with a factor −0.09. The midpoint of the thermohaline overturning is set to 5° S, in accordance with Trenberth and Caron (2001). When the density difference between south-polar and north-polar waters becomes less than 0.55 $kg\,m^{-3}$, the midpoint is shifted to 10° S. If the density difference drops below 0.51 $kg\,m^{-3}$, the midpoint is set to 15° S. This mimics the effect of relative increase of the Atlantic cross-equatorial flow. It returns to 5° S (10° S) when the density difference exceeds 0.55 $kg\,m^{-3}$ (0.51 $kg\,m^{-3}$). To obtain a better transient temperature response of the ocean, further adjustments have been made to the diffusion coefficients for the Northern Hemisphere (D_0 (north), set to $0.2 \times 10^{11}\,m^2\,yr^{-1}$), Southern Hemisphere ($D_0$ (south), set to $0.5 \times 10^{11}\,m^2\,yr^{-1}$) and vertical ocean mixing (D_z, set to $5 \times 10^3\,m^2\,yr^{-1}$). Agreement with PD observations is maintained by setting cloud optical thickness parameter τ_{cl} to 3.11 and the maximum albedo of sea ice to 0.65 (see Sect. 3.1). Table 1 summarises the alterations with respect to Bintanja (1997). Ice fraction and surface height are adjusted every 1000 years, based on the output of the Ice Sheet Model. Land fraction is considered constant in time. If, however, the ice fraction exceeds the land fraction, it is set equal to the the ice fraction. This means that all ice is considered to be ground-based, in congruence with the Ice Sheet Model. Once the ice fraction returns to smaller values, the land fraction is set back to its original value.

2.2 Ice Sheet Model

The Ice Sheet Model (ISM) consists of five hypothetical, axisymmetrical "continents", on which ice sheets can grow. These represent the five major ice sheets of the Cenozoic: the Eurasian (EuIS), North American (NaIS), Greenland (GrIS), West Antarctic (WAIS) and East Antarctic (EAIS) ice sheets. The continents are initially cone-shaped, thus being uniquely described by the height of the center (H_{cnt}) and the slope (s) of the initial bed. These quantities determine the maximum size of the ice sheet and its sensitivity to temperature (Table 2). For the GrIS, WAIS and EAIS the slopes are linear, while for the EuIS and NaIS they are parabolic, to realize better temperature sensitivity.

CPD
10, 2547–2594, 2014

Each continent has an equally-spaced grid (Table 2). It is forced by the mass balance, which is the annual sum of monthly values of accumulation minus ablation.

Because the ZEBCM does not include a hydrological scheme, accumulation is calculated internally by the ISM. It is determined as a temperature-dependent fraction of precipitation P (Bintanja et al., 2002). The precipitation parameterisation is based on the Clausius-Clapeyron equation, taking into account the fact that precipitation increases at higher temperatures (T) by 4 % per °C. Furthermore, precipitation decreases when the radius of the ice sheet (R) grows (Oerlemans, 2004):

$$P = P_0 e^{0.04T - R/R_c}. \tag{2}$$

P_0 and R_c are a reference precipitation and critical radius, chosen to match PD observations of precipitation and its sensitivity to changes in radius (Table 2).

Ablation (M) follows from an energy-balance model approach (Van den Berg et al., 2008), incorporating the effects of monthly mean temperature and local radiation (Q), varying over time:

$$M = [10T + 0.513(1-\alpha)Q + C_{abl}]/100. \tag{3}$$

Q is taken at 65° N for the EuIS and NAM, 70° N for the GrIS and 65° S for the EAIS and WAIS. C_{abl} determines the threshold for the onset of ablation. It serves as a tuning parameter for ice sheet inception (Table 2).

When the mass balance becomes positive, an ice sheet forms. The flow of the ice is then described by the continuity equation:

$$\frac{\partial H}{\partial t} = \frac{1}{r}\frac{\partial}{\partial r}(rH\overline{U}) + B, \tag{4}$$

where H is the ice thickness, r the distance from the center and $B = P - M$ the mass balance. Mean horizontal velocity ($\overline{U}$) results from the driving stresses, as obtained from the commonly used Shallow Ice Approximation (SIA) and a Weertman-type sliding velocity at the bed. Bedrock adjustment is taken into account by applying:

$$\frac{\partial b}{\partial t} = -\frac{1}{\tau_b}\left(\frac{H}{k} + b - b_0\right), \tag{5}$$

with b and b_0 the height and initial height of the bed, τ_b the relaxation time of the asthenosphere (3000 years) and $k = 3$ the ratio of the density of ice and the underlying bedrock material. A more thorough description of the ISM can be found in De Boer et al. (2010).

For this study, the height of the center H_{cnt}, slope s and ablation parameter C_{abl} are tuned in such a way that the present day sizes of Antarctica and Greenland are in accordance with the reconstruction of De Boer et al. (2010) (Table 2). Furthermore, glacial inception in East Antarctica starts when the CO_2 concentration is close to 700 ppm (at PD insolation), in accordance with DeConto et al. (2008); West Antarctica and Greenland obtain their maximum size during the Last Glacial Maximum (LGM). The North American and Eurasian ice sheets do not have a geographically imposed maximum size. The tuning parameters are chosen to ensure a total sea level drop of approximately 120 m at the LGM, and the disappearance of the North American and Eurasian ice sheet for pre-industrial conditions.

2.3 Coupling scheme

A two-way coupling of the ZEBCM and ISM is established as follows: first the ZEBCM is run for 1000 years, enough time for the atmosphere and ocean surface to adapt to the distribution of surface type and surface elevation. Thereafter, the ISM receives temperature data from the ZEBCM and is run for 1000 years. Next, the ZEBCM is forced with the new CO_2 and insolation data and the updated ice volume and height data obtained from the ISM. The mutual communication between the ZEBCM and ISM continues at 1000 year time intervals. Figure 1 illustrates the coupling scheme.

The temperature data going from the ZEBCM to the ISM consist of mean monthly atmospheric temperatures in °C (reduced to sea level), averaged over the areas where

CPD
10, 2547–2594, 2014

the ice sheets grow (Table 3). The mass balances of the Northern Hemispheric (NH) ice sheets are forced with these monthly values, corrected for height with a lapse rate of 6.5 °C km^{-1}. The volumes (V) of the different ice sheets are transferred to the ZEBCM. The relation for the volume-to-area ratio of a perfectly plastic ice sheet $V = C_{vol} \times A^{5/4}$ (Bahr et al., 1997) is then used to calculate ice extent (A). The ice sheet-dependent gain factor C_{vol} is calculated from the data of De Boer et al. (2012) (Table 3). The NH ice sheets are centered at the locations specified in Table 2 and grow circularly. The sum of the Southern Hemispheric (SH) ice sheet-areas is considered to be a single circle, centered at the South Pole (90° S).

The PD topography in the ZEBCM is taken from Becker et al. (2009). This topography is assumed to be consistent with the ice sheet heights calculated from a steady-state run of the coupled model, forced with PD insolation and pre-industrial (PI) CO_2 (280 ppm). For the NH ice sheets, height changes with respect to PI are determined from the ISM. To calculate the height changes for Antarctica, the SH ice sheets are considered to be a single perfectly plastic ice sheet. The total area is used to get the ice-sheet radius, and the ice thickness profile from the edge to the center follows from $h(x) = \sqrt{\frac{2\tau_0 x}{\rho g}}$ (Oerlemans, 2011), where $h(x)$ is the thickness at location x, τ_0 the yield stress (calculated by matching PD ice volume and PD ice area), ρ the density of ice and g the gravitational acceleration. Integration of this formula per latitude band yields the mean zonal thickness.

3 Results and discussion

3.1 Present day validation and reference experiment

First, an equilibrium PI/PD model-test was performed by running the coupled model for 100 kyr, starting with no ice, PI insolation and PI CO_2 of 280 ppm as input. After 50 kyr, the input was replaced by PD values (350 ppm CO_2). Year 50 000 represents

CPD
10, 2547–2594, 2014

the equilibrium climate for PI, year 100 000 for PD. The resulting equilibrium meridional temperature distribution for both climates is plotted and compared to PD ERA-40 reanalysis data for 1970–2000 (Uppala et al., 2005) in Fig. 2a. The difference between PI and PD temperatures is rather small: 1 K globally averaged, though locally up to 4 K. The model generally captures the observed temperature distribution and is globally averaged only slightly too warm: 288.1 K, whereas 287.7 K is observed. At 10–50° N the model produces moderately higher temperatures than the observations, while at 50–90° N they are lower. On the Southern Hemisphere, temperatures are locally somewhat overestimated at 52.5° S and 72.5° S. Local differences are most likely due to missing atmosphere and ocean dynamics. In this respect, the most important deficiency of the model is the assumption of infinite zonal exchange of energy between ocean and land atmosphere. This may lead to underestimation (overestimation) of the seasonal temperature cycle at land (ocean) dominated latitudes. Tests with finite wind strength, however, did not produce better results. The results of our model set-up, where ice volume may vary over time, are in general accordance with PD model tests performed with the old set-up of the ZEBCM, forced by observed PD ice (Bintanja, 1997). Overall, the model performs reasonably well in simulating steady-state PI and PD climate.

Hereafter, a reference run of the coupled model was performed. The model was spun up for 386 kyr, with 1072–786 kyr ago insolation data. CO_2 was gradually lowered from 730 ppm to 280 ppm. During the last 100 kyr of the spin up, an artificial interglacial-glacial CO_2 cycle was simulated by a cosine, with CO_2 values ranging from 280 ppm to 180 ppm. After the spin up, the model was run for 786 kyr. CO_2 data of the EPICA record (Jouzel et al., 2007), interpolated to yearly values, were used as input, along with 5 °-resolution insolation data of Laskar et al. (2004). The 65° N insolation and CO_2 input are plotted in Fig. 3, as well as the modeled NH temperature (40–80° N mean), sea level and global temperature. Figure 2b shows the modeled meridional temperature difference between PI and LGM (19–23 kyr ago mean), compared to the zonally-averaged data from a recent LGM reconstruction (Annan and Hargreaves (2013), [AH13]). As can be seen, the modeled distribution lies within the uncertainty band of the reconstruction

CPD
10, 2547–2594, 2014

everywhere, except at the North Pole. The modeled temperature difference gradient is larger then the reconstructed one, especially in the Northern Hemisphere. The PI-LGM global temperature difference calculated by the model is 4.9 K; this is higher than the 4.0 K found by Annan and Hargreaves (2013), but lower than the difference inferred by Schneider von Deimling et al. (2006) (5.8 K). Furthermore, the modeled PI-LGM difference is in broad agreement with results of the seven Paleoclimate Modelling Intercomparison Project Phase III (PMIP3) and Coupled Model Intercomparison Project Phase 5 (CMIP5) models, presented in the 2013 IPCC report (IPCC, 2013).

A comparison of the modeled sea level with an earlier modelling study (De Boer et al., 2010) and Red Sea sediment data (Rohling et al. (2009), [R09]) is shown in Fig. 4. In general, the glacial-interglacial cycles are simulated well by the model. There is reasonable agreement between model and data (correlation coefficient of 0.71, RMSE = 31.8 m). The last glacial cycle (125 kyr ago to present) is particularly well-modeled (correlation coefficient of 0.86, RMSE = 22.5 m). The coupled model captures the $\sim$ 40 kyr-fluctuations in sea level at 90 kyr ago and 60 kyr ago better than the model of De Boer et al. (2010). Around 330 to 260 kyr ago, modeled glaciation takes place much later than in the reconstructed sea-level record. This mismatch will be discussed further in Sect. 3.6. In most glacials, the model seems to slightly underestimate the sea level drop. This may be attributed to an underestimated sensitivity of the Antarctic ice sheets to temperature changes, resulting from the simplified geometry (De Boer et al., 2010).

3.2 Comparison of reconstructed temperatures

A comparison is made between the modeled Greenland temperature anomaly and the data reconstruction from the GRIP core (GRIP members, 1993) (Fig. 5a). The Greenland temperature is assumed to be the simulated 70° N temperature at sea level, corrected for the height of the Greenland ice sheet center. The overall agreement between model and data is decent; the model captures the main trend of the data (correlation coefficient of 0.82). The rapid, sub-millennial fluctuations, however, are not present in

CPD
10, 2547–2594, 2014

the model output because of lacking short-timescale forcing variations. Furthermore, the model seems to underestimate the amplitude of the temperature record by approximately 5 K. This is likely a consequence of the zonal averaging, which distributes temperature anomalies over the entire meridional band. In reality, local temperature differences can be much larger than the zonal average, especially over areas prone to large albedo and height changes such as Greenland.

In Fig. 5b, the modeled Antarctic temperature anomaly (60–90° S surface temperature) is shown, together with the temperature reconstruction based on the deuterium isotope record of the Dome C ice core (Jouzel et al., 2007). The modeled temperature shows rapid fluctuations of larger amplitude than the data. These are associated with shifts of the ocean-overturning midpoint. These shifts have a profound effect on Antarctic climate (see Sect. 3.3), leading to lower temperatures that are more in line with observations. However, the shifts have a discrete character as, restricted by the model resolution, the midpoint moves 5° at once. This leads to overestimation of temperature fluctuations. Nonetheless, a good coherence of model output and data is visible, both in timing (correlation coefficient of 0.73) and in amplitude (RMSE of 2.5 K). During the past four interglacials this agreement is less good; the data shows up to 4 K higher temperatures, while the model only calculates conditions similar to PI. This underestimation was also found by Ganopolski and Calov (2011), who attributed it to not including West Antarctic ice sheet changes. In our model, the West Antarctic ice sheet varies in magnitude from ~ 4 m s.l.e. during interglacials to ~ 8 m s.l.e. during glacial conditions on the one hand. On the other hand, East Antarctica increases in size by ~ 4 m s.l.e. during glacial terminations, due to increased precipitation. Therefore, the combined Antarctic ice sheet shows too little variability to produce markedly higher-than-PI interglacial temperatures. This is a consequence of the simplified geometry of the one-dimensional ice sheet model and the lack of ice shelf dynamics, as modelling studies using more sophisticated ice sheet/shelf models have shown larger-amplitude cycles of Antarctic ice-sheet size (De Boer et al., 2012; Pollard and DeConto, 2009, 2012).

CPD
10, 2547–2594, 2014

Figure 5c shows the deep-sea temperature anomaly, as calculated by the model and as reconstructed from the Mg/Ca ratio of a sediment core (Elderfield et al., 2012). The second vertical layer of the ocean model is assumed to represent the deep ocean. The sediment core was drilled as part of the Ocean Drilling Program (ODP) at 41° S (leg 181, site 1123). Two model records are displayed: the mean deep-sea temperature anomaly of the total ocean (red line), and the zonal average at 42.5° S (blue line). While the model output at 42.5° S corresponds reasonably well with the data (correlation coefficient of 0.59), the amplitude of the anomaly is smaller than observed. The aforementioned stability of the Antarctic ice sheet probably plays a role in this underestimation. Moreover, the zonally-averaged ocean is only a crude representation of the real ocean system, which has three main basins, and where local effects may amplify the deep-ocean response. Also visible in Fig. 5c is that the total ocean anomaly differs from the zonal average at 42.5° S almost solely by a scaling factor (correlation coefficient of 0.91). Deep-ocean temperatures are uniform in signal in the Southern Hemisphere, but amplified in strength at the pole, similar to atmospheric temperatures.

Studies using one-dimensional (De Boer et al., 2010) and three-dimensional (De Boer et al., 2012) ice models, have used scaling factors of 0.15 and 0.20, respectively, to relate deep-sea temperature anomalies to NH atmospheric temperature anomalies with a 3 kyr lag. Based on our model, using a scaling factor of 0.105 achieves the best fit for this relation. On the other hand, we find that a factor 0.2 is justified when the deep-sea of the same area as the atmospheric temperature (40–80° N) is considered, as can be seen in Fig. 5d (cyan and purple lines). Indeed the modeled 40–80° N deep-sea temperature anomalies have an amplitude similar to the model output of De Boer et al. (2010) (brown line). By scaling the global temperature anomalies by a factor 0.2, we obtain results similar to global deep-ocean temperature anomalies (not shown). In conclusion, a 0.2 scaling factor relates local deep-ocean temperature anomalies to local atmospheric temperature anomalies.

CPD
10, 2547–2594, 2014

3.3 Sensitivity analysis

Many assumptions and choices have been made to develop the set-up of the coupled model. Some of these may have a large impact on the model results. To test the sensitivity of the model to the aspects introduced in this study, we performed additional runs with one aspect changed at a time. Many options were tested, but most were found to be of minor importance. Here, we present the tests on the most important aspects: (1) the formulation of ocean overturning, (2) the position of the ice sheets in the ZEBCM, and (3) the radiative forcing strength of non-CO_2 greenhouse gases.

The historical strength of the NH ocean overturning is not well constrained and varies significantly between different models (e.g. Bakker et al., 2013). In our reference run, the strength is 9–11 Sv in fully glaciated conditions and 14–15 Sv during interglacials; this is similar to the range modeled by Ritz et al. (2011). A model run is performed, where the overturning circulation is fixed to its PD strength and pattern (Fig. 6; blue lines). At 620 to 500 kyr ago, glaciation is initially stronger, but ceases earlier than in the reference run. Aside from this period, the temperature and sea level reconstructions look very similar to the reference experiment. In a model run, where the overturning strength is varied, but the midpoint is fixed to its PD position (Fig. 6; black lines), the overturning strength is more stable than in the reference run. The 620 to 500 kyr ago period looks similar to the fixed PD-overturning case. This indicates that the delayed major glaciation in the reference run is caused by the shifting midpoint. In the fixed PD-overturning case NH temperatures fluctuate slightly less. This is reflected in a smaller LGM-PI temperature difference in the NH. Shifting the overturning midpoint only has a very small effect on this difference. For Antarctic temperatures, the opposite holds. Varying ocean strength increases the SH LGM-PI difference only a little, while the midpoint-shift more than doubles it.

The NH ice sheets grow circularly in the ZEBCM, starting from a fixed center. In reality, growth is more or less southward, starting at higher latitudes. The present day situation, with a matured Greenland ice sheet, but no Eurasian and North-American

CPD
10, 2547–2594, 2014

ice sheet, is accurately modeled in terms of temperature (Fig. 2a). Nonetheless, it is desirable to know the influence of the positioning of the NH ice sheets in the ZEBCM. We conduct a model run with 5° more northerly, as well as a run with 5° more southerly NH ice sheet centers. The more the ice sheets are located towards the equator, the larger the effect of increased albedo becomes, since more radiation is reflected. Consequently, temperatures are colder for more Southern ice sheet positions. Moreover, the LGM-PI temperature difference minimum shifts by 5° to 65° N (Fig. 7). As is shown in Sect. 3.4, this is caused by the surface-height changes. In contrast to the overall colder temperatures, this minimum shift can not be undone by a different tuning of the ISM. The set-up of the reference run, the Greenland ice sheet centered at 65° N and the Eurasian and North-American ice sheets at 60° N, results in the best correspondence to the LGM-PI difference found by Annan and Hargreaves (2013), while the ice sheets are still located in geographically realistic positions.

Lastly, our assumption of enhancing the radiative forcing of CO_2 with a factor 1.3, to account for non-CO_2 GHGs, is tested. When we do not enhance CO_2 radiative forcing, as expected temperature deviations are smaller (not shown). However, the simulated evolutions of the global temperature and sea level are only different from the reference reconstruction from 620 to 500 kyr ago. In this case, there is no glaciation at all during the whole period. In addition, a model run is performed, using the actual enhancement of CO_2 by CH_2 and N_2O, from records of Loulergue et al. (2008) and Spahni et al. (2005) following Köhler et al. (2010). The radiative forcing in this case is almost the same as in the reference case. Not surprisingly, there is also little difference in the reconstructed NH temperature and sea level. Even in the period 120 to 80 kyr ago, the onset of the last glacial period, where the radiative forcing is considerably stronger than in the reference, the NH ice sheets do not grow more quickly. This indicates that the build-up of ice sheets is limited by precipitation rather than the temperature decrease. As could be expected, the LGM-PI temperature difference is increased by taking non-GHGs into account (not shown). On the contrary, using a CO_2 enhancement factor

CPD
10, 2547–2594, 2014

of 1.3 has a similar effect to using real radiative forcing data of the most important non-GHGs.

3.4 Climate-ice sheet feedbacks

To quantify the effect of long-term ice-sheet variability on the climate, the fully coupled model runs are compared to (partly) uncoupled runs (Fig. 8). The ISM is still forced with ZEBCM temperatures, but no information (blue line), only surface-height change (orange line), or only ice volume (black line) is transferred back to the ZEBCM. The missing information on albedo, or surface height, or both, is prescribed as PD values. Figure 8 shows that ice sheet-climate feedbacks do not alter the evolution of global temperature fluctuations, nor do they delay glaciation. However, the amplitude of the global temperature and sea level cycles is reduced to about half the size. Temperature minima in the NH are reduced even more severely. This becomes most apparent from the LGM-PI difference, which is augmented by the ice sheet-climate to about five times the uncoupled-case difference (Fig. 9a). Ice sheet-climate feedbacks are most prominently affecting the NH. This is not surprising, since there ice sheet variability is much larger than on the SH. In Figs. 12 and 13, it is also visible that the ice-albedo feedback has a larger influence than the surface-height temperature feedback. Uncoupling ice albedo has almost the same effect as completely uncoupling the ice sheets, while climate variability is only slightly reduced by uncoupling surface height changes. Meanwhile, the distinct local minimum in the LGM-PI temperature difference at around 62.5° N is caused by surface-height changes, as it is only present in the runs with varying surface height.

A quantitative measure of the influence of ice sheets on the climate is given by the ratio of global temperature change in the fully-coupled case to that in the uncoupled-ice case (Fig. 9b; red dots). As can be seen, this ratio increases approximately linearly with the total ice amount present on Earth. A linear least-squares fit through all data points with a larger than 0.5 K global temperature decrease in the uncoupled-ice case, renders a slope of 0.04. This means that global temperature change is enhanced by 4 %

CPD
10, 2547–2594, 2014

per 10^6 km^3 of ice, which is equivalent to 1 % per 0.63 m sea level. This is mainly established by the ice-albedo feedback (Fig. 9b; black dots), rather than the surface-height temperature feedback (orange dots). In the coupled-albedo case, the enhancement percentage is 3 % (1 % per 0.84 m s.l.), while in the coupled-height it is only 0.7 % per 10^6 km^3 of ice (1 % per 3.6 m s.l.).

The effect of ice sheets on atmospheric temperature is mostly localised to the region where they grow. This is depicted by a comparison of NH to global temperature change in Figs. 9a and 9b. The ratio between the two, known as (Northern) polar amplification, is approximately constant in all cases. When ice is uncoupled, a polar amplification factor of 1.43 is deduced from a linear least-squares fit. When ice is coupled, this factor increases by 94 % to 2.78. Coupling only the ice albedo has a larger effect (factor 2.29; 60 % increase) than coupling just the surface height (factor 1.83; 28 % increase). The ice-albedo and surface-height temperature feedback also strengthen each other. This can be deduced from both the enhancement of global temperature change and polar amplification. In the case of polar amplification, the sum of their individual contributions would lead to 88 % increase, which is ~ 7 % smaller than their pooled effect.

3.5 Relative influence of CO_2 and insolation

Finally, we tested the relative contributions of CO_2 (Fig. 11) and insolation (Fig. 12), by keeping one of the variables constant in the fully-coupled set-up. Model runs are performed with insolation constant at PD value, as well as at the precession maximum value of 125 kyr ago. Additionally, we carry out three runs with constant CO_2 levels of 180 ppm (full glacial value), 230 ppm (intermediate value), and 280 ppm (interglacial value).

Neither the 280 ppm CO_2 case (Fig. 12; orange line), nor the 125 kyr ago insolation case (Fig. 11; black line), exhibit inception of the Eurasian and North-American ice sheets. This means that both variables show a threshold inception value. Likewise, both variables play a role in deglaciation, because at fixed PD insolation and at fixed 180 and

230 ppm CO_2 (Fig. 12; black and blue lines), these ice sheets do not disappear. The importance of transient effects is demonstrated by the low sea level stand of −40 m at PD, when PD insolation is used (Fig. 11; blue line). From the global temperature records of the aforementioned cases with no NH glaciation (Fig. 12; orange line, and Fig. 11; black line), it becomes clear that the effect of CO_2 is more global, than the effect of insolation. Greenhouse gases affect both hemispheres in a similar manner. In contrast, the insolation signal is dominated by precession, which effects are opposite for the two hemispheres. When the NH ice sheets are present, temperature fluctuations are much larger in both the fixed CO_2 and the fixed insolation cases, because of the ice sheet-climate feedbacks. Insolation affects ice volume both indirectly, through temperature in the ZEBCM, and directly, through the mass balance in the ISM (Eq. 3). The indirect effect is more important, as fixing only the ISM input has almost no effect (not shown). The reference sea level is correlated more strongly to CO_2 (coefficient of 0.84) than to insolation (coefficient of 0.35). This indicates that CO_2 levels provide the envelope of sea level. Insolation changes have a damping or amplifying effect, as well as being decisive for the timing of glacial inception. In this analysis, insolation and CO_2 are considered as separate forcings, while in reality CO_2 levels are part of the Earth's system response to external forcings (e.g. through the chemical weathering feedback (Walker et al., 1981)).

3.6 Discussion

By using an energy balance climate model coupled to a one-dimensional ice-sheet model, we reconstructed global mean sea level and a zonally-averaged air temperature over the past 800 kyr. The sensitivity tests presented in Sect. 3 show that SH temperature is largely dependent on the parameterisation of the ocean overturning. In contrast, NH temperature and sea level are affected less and are more robust. Furthermore, the influence of non-CO_2 GHGs is shown to be very important for the strength of glaciation. They largely determine the amplitude of sea level fall during the whole reconstructed period. However, the reconstructed temporal evolution of temperature and

CPD
10, 2547–2594, 2014

sea level are only affected in the period 620 to 500 kyr ago. During this period, glaciation relies on sufficiently low NH temperatures, generated by both non-CO_2 forcing and ocean overturning. Multiplying the radiative forcing of CO_2 with the mean amplification over the past 800 kyr (factor of 1.3) according to Köhler et al. (2010), has to a large degree the same impact as explicitly modelling non-CO_2 GHG forcing. Finally, the sensitivity analysis shows only a minor influence of the position of the ice sheets in the ZEBCM with respect to the resulting temperature and sea level reconstruction.

The set-up in this study is chosen to ensure that the simulated global sea level is in the best possible accordance with the Red Sea record of Rohling et al. (2009), and the modeled temperature difference between LGM and PD agrees within uncertainty limits with the data reconstruction provided by Annan and Hargreaves (2013). Overall, the modeled sea level is in reasonable agreement with the data, except at around 330 to 260 kyr ago. During this period, NH glaciation is simulated much later than in the data record. This is most likely a consequence of large hysteresis in the ISM induced by the simplified geometry. If Eurasia and North America are deglaciated entirely in the model, glacial inception on the NH only takes place when a drop in CO_2 is accompanied by a large enough drop in NH summer insolation. This is demonstrated by separate hysteresis tests, where CO_2 is decreased in steps of 10 ppm per 30 kyr from 280 ppm to 180 ppm and then increased in reversed manner. Insolation is kept at constant level of 335 (high NH summer insolation), 326 (intermediate) and 325 (low) kyr ago. In the reference case (REF), it is first decreased in steps of 1 kyr from the high to the low extreme, and then increased back to the initial level, in phase with CO_2. An index is assigned to the input values, linearly ranging from favourable –180 ppm CO_2 (and low NH summer insolation for REF); index 0 – to unfavourable –280 ppm CO_2 (and high NH summer insolation for REF); index 1 – for NH glaciation. Comparing the reference case to the fixed-insolation cases, it is apparent that hysteresis is reduced when NH summer insolation and CO_2 are in phase (Fig. 13). A more realistic topography than used here would ensure that some high parts remain glaciated (or at least glaciate much earlier), and cause a positive feedback when the CO_2 level decreases, thereby reducing the

CPD
10, 2547–2594, 2014

hysteresis. Due to high CO_2 and summer insolation in the NH, the Eurasian and North American ice sheets totally disappear at 334 kyr ago. During the period 334 to 280 kyr ago, NH summer insolation does not drop to low enough levels to realize inception. This only occurs at 280 kyr ago, when the CO_2 level is very low. The NH ice sheets then grow quickly, because of the low CO_2 levels and the ice sheet-climate feedbacks. Although it cannot be excluded that the importance of radiation is overestimated in our model, it only leads to a model-data mismatch from 334 to 280 kyr ago. Removing this period from our data analysis does not significantly alter the resulting strength of the ice sheet-climate feedbacks (4 % per 10^6 km^3 of ice) and polar amplification factor (2.78), which we consider our most important findings.

As mentioned before, land ice has an influence on climate through albedo and surface height. However, the complete temperature response to land ice is also determined by changing sea-ice and snow cover, which are fast feedbacks. To quantify this influence we did two further runs of the model with sea-ice and snow cover kept constant; one with coupled ice sheets, and one with land-ice cover and surface height fixed at PD levels (Table 4). Compared to the completely-fixed run, coupling land ice leads to an increase of global temperature anomalies by 0.7 % per 10^6 km^3 of ice (1 % per 3.6 m s.l.). Coupling only sea-ice and snow (the land-ice fixed case) increases global temperature anomalies by 2.2 % per 10^6 km^3 of ice (1 % per 1.2 m s.l.). Land-ice cover is taken from the ISM output, which is in this case not used to force the ZEBCM. Therefore, the effect of including only fast ice feedbacks, is more than three times as important as the effect of including only land-ice changes. The true importance of the land ice feedback only appears when we compare the fully coupled results to those of the completely-fixed run. The temperature anomalies are then increased by 5.2 % per 10^6 km^3 of ice (1 % per 0.48 m s.l.), implying that the temperature response is more than twice as large then for the case where only the sea-ice and snow variation are taken into account. This result is much larger than the product of the separate effects, which is caused by positive reinforcement of the effect of land ice, and sea ice and snow, on atmospheric temperature.

CPD
10, 2547–2594, 2014

Interaction of ice sheets and climate during the past 800 000 years

L. B. Stap et al.

Our modeled polar amplification of the LGM-PI surface air temperature difference is within uncertainty range consistent with a recent LGM data reconstruction (Annan and Hargreaves, 2013), and the results of seven models presented in the 2013 IPCC report (IPCC, 2013). Using a GCM, Singarayer and Valdes (2010) performed two tests on polar amplification over the past 120 kyr. In one, they varied insolation and CO_2, but kept surface elevation and ice extent at PD levels. In the other, insolation and CO_2 were still varied, but they used the ice sheet reconstruction of Peltier and Fairbanks (2006) to force their model. Both in the coupled and uncoupled ice case, the ratio of Greenland temperature change to global temperature change corresponds to our results. In the uncoupled-ice case, our meridional LGM-PI temperature difference distribution, normalised by global temperature change, is also in broad agreement with the results of an ensemble of GCMs (Holland and Bitz, 2003). Although they based their distribution on the difference induced by a doubling of CO_2 with respect to PD (keeping ice sheets constant at PD size), the results are comparable because of the normalisation. Our model shows an ~2.2 times global warming temperature difference at the North Pole; this is within the 1.5 to 4.5 times amplification range in Holland and Bitz (2003). The agreement with these results, obtained with more sophisticated models, provides confidence in our resulting polar amplification factors.

4 Summary and conclusion

We have coupled a Zonally averaged Energy Balance Climate Model (ZEBCM) to a one-dimensional Ice Sheet Model (ISM). The coupled model was used to obtain a 800 000 year record of meridional atmospheric and ocean temperature, and global eustatic sea level. The sea level record was tuned to match a Red Sea sediment data reconstruction (Rohling et al., 2009) as closely as possible, with a correlation coefficient of 0.71 and a RMSE of 31.8 m. The simulated Antarctic temperature, Greenland temperature and deep-sea temperature are in reasonable agreement with proxy-data reconstructions. Our model shows that NH polar temperatures are mainly determined

CPD
10, 2547–2594, 2014

by the waxing and waning of the Eurasian and North-American ice sheets, while the Antarctic ice sheet is more stable and SH climate is heavily influenced by the strength of ocean overturning. We realize that all our results are model specific and only large-scale features are significant, because of limitations imposed by the zonal averaging and rather coarse resolution (5°) of the ZEBCM and the lack of detailed physics. Furthermore, the ISM has a highly simplified geometry and misses ice shelf dynamics. However, this study significantly improves on earlier stand-alone ISM results, forced by an inverse δ^{18}O routine (De Boer et al., 2010). By including the ZEBCM, a more comprehensive view of global climate is acquired, as it is no longer an anomaly with respect to the PD climate. Now, we do not only calculate the meridional temperature distribution, but also more realistic deep-sea temperatures. Deep-sea temperature fluctuations are tightly coupled to fluctuations of atmospheric temperatures in the same region, reduced by a factor 5 approximately. Switching CO_2 and insolation forcing on and off, enabled us to study the relative influence of these two variables. Atmospheric temperature on the NH is controlled by a complex interaction of CO_2 and insolation. Both variables, as well as transient effects, govern the evolution of ice sheets on the Northern Hemisphere. By comparing the fully-coupled results to results from the ZEBCM forced with PD albedo and/or surface height, we have quantified the importance of the ice-albedo feedback and the surface-height temperature feedback. The combined long-term ice sheet-climate feedback amplifies global temperature anomalies from PI with 4 % per 10^6 km^3 of ice (1 % per 0.63 m s.l.). In full glacial conditions ($\sim 40 \times 10^6$ km^3 of ice), this leads to a factor 2.6 increase in the temperature change. Furthermore, it almost doubles polar amplification, from 1.43 to 2.78. The dominant feedback is the ice-albedo feedback, while the surface-height temperature feedback has only minor influence. Compared to the results of a model run where also the fast ice feedbacks (sea ice and snow) are fixed, the amplification factor of global temperature anomalies increases to 5.2 % per 10^6 km^3 of ice (1 % per 0.48 m s.l.) in the fully-coupled run. This is more than twice as large as the effect of only including sea-ice and snow cover variation (2.2 % per 10^6 km^3 of ice or 1 % per 1.2 m s.l.).

CPD
10, 2547–2594, 2014

In future research, the use of the coupled model will be extended into the Pliocene (5 Myr ago to PD), and the Early to Middle Miocene (23 to 13 Myr ago). During the former period, the Antarctic ice sheet was more variable in size, while the latter period is characterized by glaciations and deglaciations of the Northern Hemisphere. A marine benthic δ^{18}O-isotope model will be incorporated, to allow for an independent comparison with paleo proxy-records (Lisiecki and Raymo, 2005; Zachos et al., 2008; Cramer et al., 2009).

Acknowledgements. Financial support was provided by the Netherlands Organization of Scientific Research (NWO). We thank James Annan and Eric Tuenter for sharing their data.

References

Abe-Ouchi, A., Saito, F., Kawamura, K., Raymo, M. E., Okuno, J., Takahashi, K., and Blatter, H.: Insolation-driven 100,000-year glacial cycles and hysteresis of ice-sheet volume, Nature, 500, 190–193, 2013. 2550, 2551

Annan, J. D. and Hargreaves, J. C.: A new global reconstruction of temperature changes at the Last Glacial Maximum, Clim. Past, 9, 367–376, doi:10.5194/cp-9-367-2013, 2013. 2549, 2558, 2559, 2563, 2567, 2569, 2583

Bahr, D. B., Meier, M. F., and Peckham, S. D.: The physical basis of glacier volume-area scaling, J. Geophys. Res.-Sol. Ea., 102, 20355–20362, 1997. 2557

Bakker, P., Stone, E. J., Charbit, S., Gröger, M., Krebs-Kanzow, U., Ritz, S. P., Varma, V., Khon, V., Lunt, D. J., Mikolajewicz, U., Prange, M., Renssen, H., Schneider, B., and Schulz, M.: Last interglacial temperature evolution – a model inter-comparison, Clim. Past, 9, 605–619, doi:10.5194/cp-9-605-2013, 2013. 2562

Becker, J. J., Sandwell, D. T., Smith, W. H. F., Braud, J., Binder, B., Depner, J., Fabre, D., Factor, J., Ingalls, S., Kim, S. H., Ladner, R., Marks, K., Nelson, S., Pharaoh, A., Trimmer, R., Von Rosenberg, J., Wallace, G., and Weatherall, P.: Global bathymetry and elevation data at 30 arc seconds resolution: SRTM30PLUS, Mar. Geod., 32, 355–371, doi:10.1080/01490410903297766, 2009. 2557

Bintanja, R.: The Antarctic Ice Sheet and Climate, Ph.D. thesis, Utrecht University, Utrecht, the Netherlands, 1995. 2553

Bintanja, R.: The parameterization of shortwave and longwave radiative fluxes for use in zonally averaged climate models, J. Climate, 9, 439–454, 1996. 2552
Bintanja, R.: Sensitivity experiments performed with an energy balance atmosphere model coupled to an advection–diffusion ocean model, Theor. Appl. Climatol., 56, 1–24, 1997. 2551, 2552, 2553, 2554, 2558, 2578
Bintanja, R. and Oerlemans, J.: The effect of reduced ocean overturning on the climate of the last glacial maximum, Clim. Dynam., 12, 523–533, 1996. 2553
Bintanja, R. and Van de Wal, R. S. W.: North American ice-sheet dynamics and the onset of 100,000-year glacial cycles, Nature, 454, 869–872, 2008. 2550
Bintanja, R., Van de Wal, R. S. W., and Oerlemans, J.: Global ice volume variations through the last glacial cycle simulated by a 3-D ice-dynamical model, Quatern. Int., 95, 11–23, 2002. 2555
Bintanja, R., van de Wal, R. S. W., and Oerlemans, J.: Modelled atmospheric temperatures and global sea levels over the past million years, Nature, 437, 125–128, 2005. 2550
Cramer, B., Toggweiler, J., Wright, J., Katz, M., and Miller, K.: Ocean overturning since the Late Cretaceous: Inferences from a new benthic foraminiferal isotope compilation, Paleoceanography, 24, PA4216, doi:10.1029/2008PA001683, 2009. 2571
Dahl-Jensen, D., Albert, M. R., Aldahan, A., Azuma, N., Balslev-Clausen, D., Baumgartner, M., Berggren, A.-M., Bigler, M., Binder, T., Blunier, T., Bourgeois, J. C., Brook, E. J., Buchardt, S. L., Buizert, C., Capron, E., Chappellaz, J., Chung, J., Clausen, H. B., Cvijanovic, I., Davies, S. M., Ditlevsen, P., Eicher, O., Fischer, H., Fisher, D. A., Fleet, L. G., Gfeller, G., Gkinis, V., Gogineni, S., Goto-Azuma, K., Grinsted, A., Gudlaugsdottir, H., Guillevic, M., Hansen, S. B., Hansson, M., Hirabayashi, M., Hong, S., Hur, S. D., Huybrechts, P., Hvidberg, C. S., Iizuka, Y., Jenk, T., Johnsen, S. J., Jones, T. R., Jouzel, J., Karlsson, N. B., Kawamura, K., Keegan, K., Kettner, E., Kipfstuhl, S., Kjaer, H. A., Koutnik, M., Kuramoto, T., Koehler, P., Laepple, T., Lais, A., Langen, P. L., Larsen, L. B., Leuenberger, D., Leuenberger, M., Leuschen, C., Li, J., Lipenkov, V., Martinerie, P., Maselli, O. J., Masson-Delmotte, V., McConnell, J. R., Miller, H., Mini, O., Miyamoto, A., Montagnat-Rentier, M., Mulvaney, R., Muscheler, R., Orsi, A. J., Paden, J., Panton, C., Pattyn, F., Petit, J.-R., Pol, K., Popp, T., Possnert, G., Prie, F., Prokopiou, M., Quiquet, A., Rasmussen, S. O., Raynaud, D., Ren, J., Reutenauer, C., Ritz, C., Rockmann, T., Rosen, J. L., Rubino, M., Rybak, O., Samyn, D., Sapart, C. J., Schilt, A., Schmidt, A. M. Z., Schwer, J., Schuepbach, S., Seierstad, I., Dahl-Jensen, D., Albert, M. R., Aldahan, A., Azuma, N., Balslev-Clausen, D., Baumgartner, M., Berggren, A.-M., Bigler, M.,

CPD
10, 2547–2594, 2014

Binder, T., Blunier, T., Bourgeois, J. C., Brook, E. J., Buchardt, S. L., Buizert, C., Capron, E., Chappellaz, J., Chung, J., Clausen, H. B., Cvijanovic, I., Davies, S. M., Ditlevsen, P., Eicher, O., Fischer, H., Fisher, D. A., Fleet, L. G., Gfeller, G., Gkinis, V., Gogineni, S., Goto-Azuma, K., Grinsted, A., Gudlaugsdottir, H., Guillevic, M., Hansen, S. B., Hansson, M., Hirabayashi, M., Hong, S., Hur, S. D., Huybrechts, P., Hvidberg, C. S., Iizuka, Y., Jenk, T., Johnsen, S. J., Jones, T. R., Jouzel, J., Karlsson, N. B., Kawamura, K., Keegan, K., Kettner, E., Kipfstuhl, S., Kjaer, H. A., Koutnik, M., Kuramoto, T., Koehler, P., Laepple, T., Lais, A., Langen, P. L., Larsen, L. B., Leuenberger, D., Leuenberger, M., Leuschen, C., Li, J., Lipenkov, V., Martinerie, P., Maselli, O. J., Masson-Delmotte, V., McConnell, J. R., Miller, H., Mini, O., Miyamoto, A., Montagnat-Rentier, M., Mulvaney, R., Muscheler, R., Orsi, A. J., Paden, J., Panton, C., Pattyn, F., Petit, J.-R., Pol, K., Popp, T., Possnert, G., Prie, F., Prokopiou, M., Quiquet, A., Rasmussen, S. O., Raynaud, D., Ren, J., Reutenauer, C., Ritz, C., Rockmann, T., Rosen, J. L., Rubino, M., Rybak, O., Samyn, D., Sapart, C. J., Schilt, A., Schmidt, A. M. Z., Schwer, J., Schuepbach, S., and Seierstad, I.: Eemian interglacial reconstructed from a Greenland folded ice core, Nature, 493, 489–494, 2013. 2549

De Boer, B., Van de Wal, R. S. W., Bintanja, R., Lourens, L. J., and Tuenter, E.: Cenozoic global ice-volume and temperature simulations with 1-D ice-sheet models forced by benthic $\delta^{18}O$ records, Ann. Glaciol., 51, 23–33, 2010. 2550, 2551, 2556, 2559, 2561, 2570, 2585, 2586

De Boer, B., Van de Wal, R., Lourens, L., Bintanja, R., and Reerink, T.: A continuous simulation of global ice volume over the past 1 million years with 3-D ice-sheet models, Clim. Dynam., 1–20, doi:10.1007/s00382-012-1562-2, 2012. 2550, 2557, 2560, 2561

DeConto, R. M. and Pollard, D.: Rapid Cenozoic glaciation of Antarctica induced by declining atmospheric CO_2, Nature, 421, 245–249, 2003. 2551

DeConto, R. M., Pollard, D., Wilson, P. A., Pälike, H., Lear, C. H., and Pagani, M.: Thresholds for Cenozoic bipolar glaciation, Nature, 455, 652–656, 2008. 2556

Elderfield, H., Ferretti, P., Greaves, M., Crowhurst, S., McCave, I., Hodell, D., and Piotrowski, A.: Evolution of ocean temperature and ice volume through the Mid-Pleistocene climate transition, Science, 337, 704–709, 2012. 2561, 2586

EPICA community members: Eight glacial cycles from an Antarctic ice core, Nature, 429, 623–628, 2004. 2549

EPICA community members: One-to-one coupling of glacial climate variability in Greenland and Antarctica, Nature, 444, 195–198, 2006. 2549

CPD
10, 2547–2594, 2014

Ganopolski, A. and Calov, R.: The role of orbital forcing, carbon dioxide and regolith in 100 kyr glacial cycles, Clim. Past, 7, 1415–1425, doi:10.5194/cp-7-1415-2011, 2011. 2550, 2551, 2560

Ganopolski, A., Calov, R., and Claussen, M.: Simulation of the last glacial cycle with a coupled climate ice-sheet model of intermediate complexity, Clim. Past, 6, 229–244, doi:10.5194/cp-6-229-2010, 2010. 2551

Gill, A. E.: Atmosphere–Ocean Dynamics, vol. 30, Academic Press, 1982. 2553

GRIP members: Climate instability during the last interglacial period recorded in the GRIP ice core, Nature, 364, 203–207, 1993. 2549, 2559, 2586

Helsen, M. M., van de Berg, W. J., van de Wal, R. S. W., van den Broeke, M. R., and Oerlemans, J.: Coupled regional climate–ice-sheet simulation shows limited Greenland ice loss during the Eemian, Clim. Past, 9, 1773–1788, doi:10.5194/cp-9-1773-2013, 2013. 2551

Herrington, A. R. and Poulsen, C. J.: Terminating the Last Interglacial: the role of ice sheet-climate feedbacks in a GCM asynchronously coupled to an ice sheet model, J. Climate, 25, 1871–1882, 2011. 2551

Holland, M. M. and Bitz, C. M.: Polar amplification of climate change in coupled models, Clim. Dynam., 21, 221–232, 2003. 2569

IPCC: Climate Change 2013: The Physical Science Basis. Contribution of Working Group I to the Fifth Assessment Report of the Intergovernmental Panel on Climate Change edited by: Stocker, T. F., Qin, D., Plattner, G.-K., Tignor, M., Allen, S. K., Boschung, J., Nauels, A., Xia, Y., Bex, V., and Midgley, P. M., Cambridge University Press, Cambridge, UK and New York, NY, USA, 2013. 2553, 2559, 2569

Jouzel, J., Masson-Delmotte, V., Cattani, O., Dreyfus, G., Falourd, S., Hoffmann, G., Minster, B., Nouet, J., Barnola, J. M., Chappellaz, J., Fischer, H., Gallet, J. C., Johnsen, S., Leuenberger, M., Loulergue, L., Luethi, D., Oerter, H., Parrenin, F., Raisbeck, G., Raynaud, D., Schilt, A., Schwander, J., Selmo, E., Souchez, R., Spahni, R., Stauffer, B., Steffensen, J. P., Stenni, B., Stocker, T. F., Tison, J. L., Werner, M., and Wolff, E. W.: Orbital and millennial Antarctic climate variability over the past 800,000 years, Science, 317, 793–796, 2007. 2549, 2553, 2558, 2560, 2584, 2586

Köhler, P., Bintanja, R., Fischer, H., Joos, F., Knutti, R., Lohmann, G., and Masson-Delmotte, V.: What caused Earth's temperature variations during the last 800,000 years? Data-based evidence on radiative forcing and constraints on climate sensitivity, Quaternary Sci. Rev., 29, 129–145, 2010. 2549, 2553, 2563, 2567

Langebroek, P. M., Paul, A., and Schulz, M.: Antarctic ice-sheet response to atmospheric CO_2 and insolation in the Middle Miocene, Clim. Past, 5, 633–646, doi:10.5194/cp-5-633-2009, 2009. 2551

Laskar, J., Robutel, P., Joutel, F., Gastineau, M., Correia, A., and Levrard, B.: A long-term numerical solution for the insolation quantities of the Earth, Astron. Astrophys., 428, 261–285, 2004. 2553, 2558, 2584

Lisiecki, L. E. and Raymo, M. E.: A Pliocene–Pleistocene stack of 57 globally distributed benthic $\delta^{18}O$ records, Paleoceanography, 20, PA1003, doi:10.1029/2004PA001071, 2005. 2549, 2571

Loulergue, L., Schilt, A., Spahni, R., Masson-Delmotte, V., Blunier, T., Lemieux, B., Barnola, J.-M., Raynaud, D., Stocker, T. F., and Chappellaz, J.: Orbital and millennial-scale features of atmospheric CH_4 over the past 800,000 years, Nature, 453, 383–386, 2008. 2549, 2563

Myhre, G., Highwood, E. J., Shine, K. P., and Stordal, F.: New estimates of radiative forcing due to well mixed greenhouse gases, Geophys. Res. Lett., 25, 2715–2718, 1998. 2553

NGRIP members: High-resolution record of Northern Hemisphere climate extending into the last interglacial period, Nature, 431, 147–151, 2004. 2549

North, G. R.: Theory of energy-balance climate models, J. Atmos. Sci., 32, 2033–2043, 1975. 2552

Oerlemans, J.: Antarctic ice volume and deep-sea temperature during the last 50 Myr: a model study, Ann. Glaciol., 39, 13–19, 2004. 2555

Oerlemans, J.: Minimal Glacier Models (2nd print), Igitur, Utrecht Publishing & Archiving Services, Utrecht, the Netherlands, 2011. 2557

Paillard, D. and Parrenin, F.: The Antarctic ice sheet and the triggering of deglaciations, Earth Planet. Sc. Lett., 227, 263–271, 2004. 2550

Peltier, W. and Fairbanks, R. G.: Global glacial ice volume and Last Glacial Maximum duration from an extended Barbados sea level record, Quaternary Sci. Rev., 25, 3322–3337, 2006. 2569

Pollard, D. and DeConto, R. M.: Modelling West Antarctic ice sheet growth and collapse through the past five million years, Nature, 458, 329–332, 2009. 2560

Pollard, D. and DeConto, R. M.: A simple inverse method for the distribution of basal sliding coefficients under ice sheets, applied to Antarctica, The Cryosphere, 6, 953–971, doi:10.5194/tc-6-953-2012, 2012. 2560

Pollard, D., Kump, L., and Zachos, J.: Interactions between carbon dioxide, climate, weathering, and the Antarctic ice sheet in the earliest Oligocene, Global Planet. Change, 111, 258–267, 2013. 2551

Ridley, J. K., Huybrechts, P., Gregory, J., and Lowe, J.: Elimination of the Greenland ice sheet in a high CO_2 climate, J. Climate, 18, 3409–3427, 2005. 2551

Ritz, S. P., Stocker, T. F., and Joos, F.: A coupled dynamical ocean-energy balance atmosphere model for paleoclimate studies, J. Climate, 24, 349–375, 2011. 2550, 2553, 2562

Rohling, E., Grant, K., Bolshaw, M., Roberts, A., Siddall, M., Hemleben, C., and Kucera, M.: Antarctic temperature and global sea level closely coupled over the past five glacial cycles, Nat. Geosci., 2, 500–504, 2009. 2549, 2559, 2567, 2569, 2585

Schmittner, A., Urban, N. M., Shakun, J. D., Mahowald, N. M., Clark, P. U., Bartlein, P. J., Mix, A. C., and Rosell-Melé, A.: Climate sensitivity estimated from temperature reconstructions of the Last Glacial Maximum, Science, 334, 1385–1388, 2011. 2549

Schneider von Deimling, T., Ganopolski, A., Held, H., and Rahmstorf, S.: How cold was the last glacial maximum?, Geophys. Res. Lett., 33, L14709, doi:10.1029/2006GL026484, 2006. 2549, 2559

Singarayer, J. S. and Valdes, P. J.: High-latitude climate sensitivity to ice-sheet forcing over the last 120 kyr, Quaternary Sci. Rev., 29, 43–55, 2010. 2569

Spahni, R., Chappellaz, J., Stocker, T. F., Loulergue, L., Hausammann, G., Kawamura, K., Flückiger, J., Schwander, J., Raynaud, D., Masson-Delmotte, V., and Jouzel, J.: Atmospheric methane and nitrous oxide of the late Pleistocene from Antarctic ice cores, Science, 310, 1317–1321, 2005. 2549, 2563

Trenberth, K. E. and Caron, J. M.: Estimates of meridional atmosphere and ocean heat transports, J. Climate, 14, 3433–3443, 2001. 2554

Uppala, S. M., Kållberg, P. W., Simmons, A. J., Andrae, U., Da Costa Bechtold, V., Fiorino, M., Gibson, J. K., Haseler, J., Hernandez, A., Kelly, G. A., Li, X., Onogi, K., Saarinen, S., Sokka, N., Allan, R. P., Andersson, E., Arpe K., Balmaseda, M. A., Beljaars, A. C. M., Van de Berg, L., Bidlot, J., Bormann, N., Caires, S., Chevallier, F., Dethof, A., Dragosavac, M., Fisher, M., Fuentes, M., Hagemann, S., Hólm, E., Hoskins, B. J., Isaksen, L., Janssen, P. A. E. M., Jenne, R., McNally, A. P., Mahfouf, J. F., Morcrette, J.-J., Rayner, N. A., Saunders, R. W., Simon, P., Sterl, A., Trenberth, K. E., Untch, A., Vasiljevic, D., Viterbo, P., and Woollen, J.: The ERA-40 re-analysis, Q. J. Roy. Meteor. Soc., 131, 2961–3012, 2005. 2558, 2583

CPD
10, 2547–2594, 2014

van de Wal, R. S. W., de Boer, B., Lourens, L. J., Köhler, P., and Bintanja, R.: Reconstruction of a continuous high-resolution CO_2 record over the past 20 million years, Clim. Past, 7, 1459–1469, doi:10.5194/cp-7-1459-2011, 2011. 2551

Van den Berg, J., van de Wal, R. S. W., and Oerlemans, J.: A mass balance model for the Eurasian ice sheet for the last 120,000 years, Global Planet. Change, 61, 194–208, 2008. 2555

Walker, J. C., Hays, P., and Kasting, J. F.: A negative feedback mechanism for the long-term stabilization of Earth's surface temperature, J. Geophys. Res.-Oceans, 86, 9776–9782, 1981. 2566

Wilson, D. S., Pollard, D., DeConto, R. M., Jamieson, S. S., and Luyendyk, B. P.: Initiation of the West Antarctic Ice Sheet and estimates of total Antarctic ice volume in the earliest Oligocene, Geophys. Res. Lett., 40, 4305–4309, 2013. 2551

Zachos, J. C., Dickens, G. R., and Zeebe, R. E.: An early Cenozoic perspective on greenhouse warming and carbon-cycle dynamics, Nature, 451, 279–283, 2008. 2549, 2571

CPD

10, 2547–2594, 2014

Interaction of ice sheets and climate during the past 800 000 years

L. B. Stap et al.

Table 1. Model parameters for the ZEBCM, altered in this study (new value) with respect to Bintanja (1997) (old value).

Parameter	Description	Old value	New value
	Radiative forcing per CO_2-doubling ($W\,m^{-2}$)	3.5	3.7
	Enhancement of CO_2 radiative forcing by other GHGs (%)	–	30
D_0 (north)	Diffusion coefficient for the Northern Hemisphere ($m^2\,yr^{-1}$)	4.0×10^{11}	2.0×10^{10}
D_0 (south)	Diffusion coefficient for the Southern Hemisphere ($m^2\,yr^{-1}$)	1.0×10^{11}	0.5×10^{11}
D_z	Diffusion coefficient for vertical ocean mixing ($m^2\,yr^{-1}$)	2.0×10^3	5.0×10^3
τ_{cl}	Cloud optical thickness parameter	3.11	3.5
α_{SI}	Maximum albedo of sea ice	0.75	0.65

CPD
10, 2547–2594, 2014
Interaction of ice sheets and climate during the past 800 000 years
L. B. Stap et al.

CPD
10, 2547–2594, 2014

Interaction of ice sheets and climate during the past 800 000 years

L. B. Stap et al.

Table 2. Model parameters for the ISM.

Parameter	Description	EuIS	NaIS	GrIS	EAIS	WAIS
H_{cnt}	Height of the center (m)	1400	1400	800	1450	400
s	Slope of the initial bed	−0.0000165*	−0.000016*	−0.0014	−0.0010	−0.0011
N_{grid}	Number of grid points	100	100	100	120	100
Δl	Grid size (km)	25	25	15	20	15
P_0	Uncorr. prec. (m yr^{-1})	0.88	1.15	1.34	0.71	1.37
R_c	Critical radius (km)	1500	1800	750	2000	700
C_{abl}	Ablation parameter	−51	−41	−48	−30	−5
ΔS_{PD}	PD ice volume (m.s.l.)	0	0	7	56	7

* Parabolic profile, value given in m^{-1}.

CPD
10, 2547–2594, 2014

Table 3. Values used for the data transfer from the ZEBCM to the ISM and vice versa. Note that in the ZEBCM, East and West Antarctica are combined to one ice sheet.

Ice Sheet	Area of temperature input for ISM	Location of center in ZEBCM	Value of C_{vol}
Eurasian	40–80° N	65° N	0.92
North American	40–80° N	65° N	0.79
Greenland	72.5° N	70° N	1.20
East Antarctica	65–90° S	90° S	0.85
West Antarctica	65–90° S	90° S	0.85

Table 4. Overview of the enhancement of global temperature anomalies induced by coupling the land ice and/or freely calculating sea-ice and snow cover in the ZEBCM, relative to the completely fixed run where PD values are prescribed.

Run	land ice	sea ice, snow	Enhancement of ΔT_{glob} rel. to fixed (% per 10^6 km^3 of ice)
completely fixed	fixed	fixed	–
slow feedbacks only	coupled	fixed	0.7
fast feedbacks only	fixed	free	2.2
coupled	coupled	free	5.2

CPD
10, 2547–2594, 2014

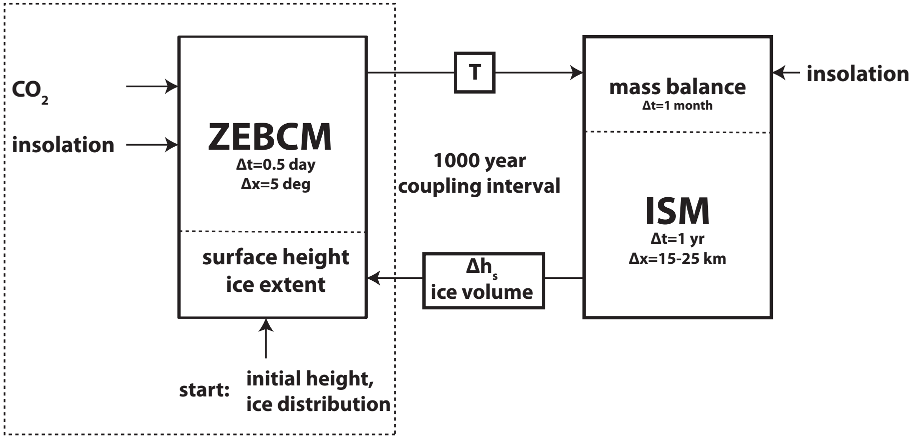

Figure 1. Schematic overview of the coupling between the Zonally averaged Energy Balance Climate Model (ZEBCM) and the Ice Sheet Model (ISM). The novel aspect of this study is marked by a dashed box.

CPD
10, 2547–2594, 2014

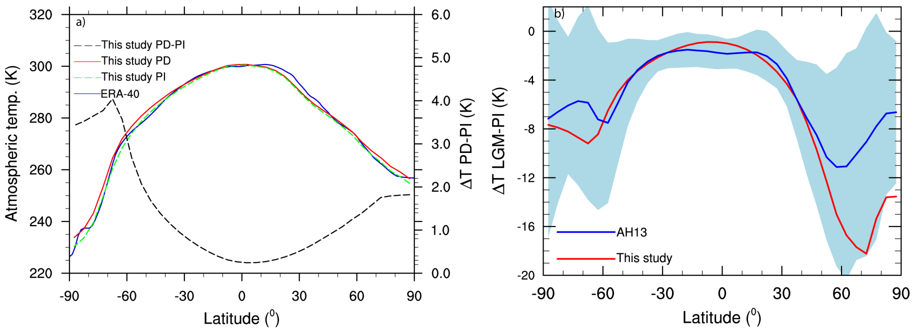

Figure 2. (a) Modeled PI (dashed green) and PD (red) atmospheric meridional temperature distributions and PD ERA-40 reanalysis data(Uppala et al., 2005; blue). **(b)** Modeled reference LGM-PI atmospheric temperature difference (red), compared to the data reconstruction of Annan and Hargreaves (2013) ([AH13]; blue, with error bars).

CPD
10, 2547–2594, 2014

Interaction of ice sheets and climate during the past 800 000 years

L. B. Stap et al.

Title Page
Abstract Introduction
Conclusions References
Tables Figures
Back Close
Full Screen / Esc
Printer-friendly Version
Interactive Discussion

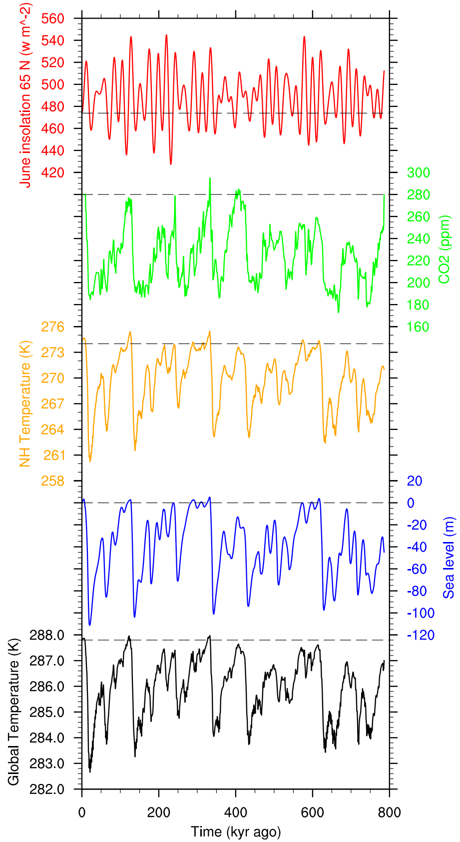

Figure 3. Insolation (Laskar et al., 2004; red) and CO_2 (Jouzel et al., 2007; green) input, and modeled reference NH temperature (orange), sea level relative to PD (blue), and global temperature (black).

CPD
10, 2547–2594, 2014

Interaction of ice sheets and climate during the past 800 000 years

L. B. Stap et al.

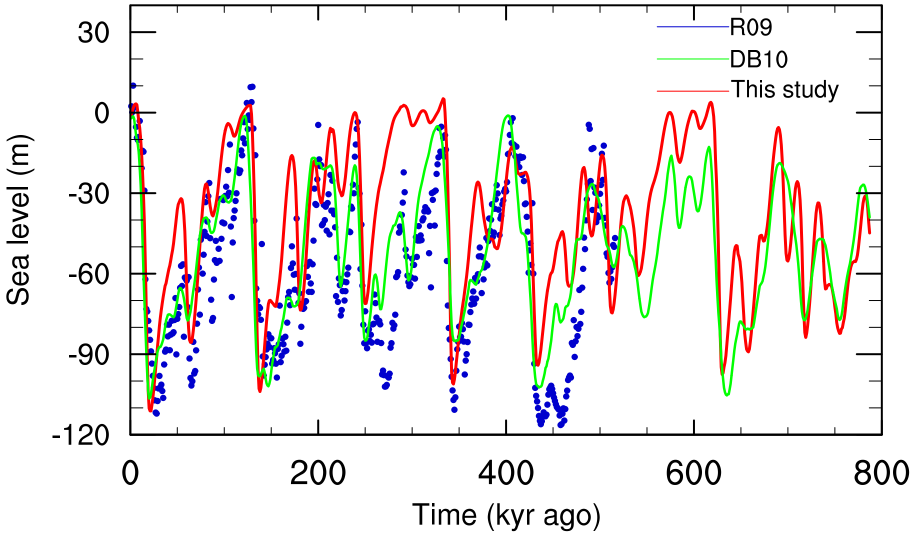

Figure 4. Modeled reference sea level relative to PD (red), compared to data from Red Sea sediments (Rohling et al., 2009; blue dots) and model output from De Boer et al. (2010) (green).

CPD
10, 2547–2594, 2014

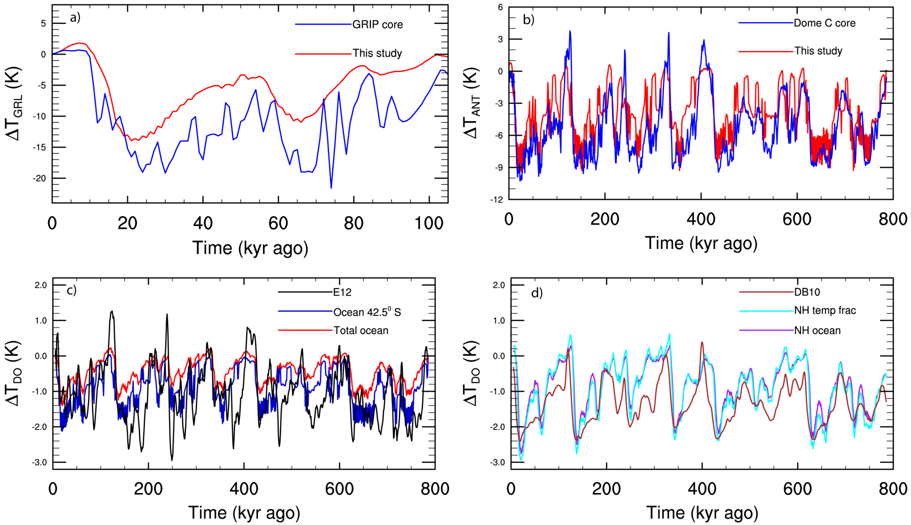

Figure 5. (a) Modeled reference Greenland temperature anomaly from PI (red), compared to a data reconstruction from the GRIP core (GRIP members, 1993; blue). **(b)** Modeled reference Antarctic temperature anomaly from PI (red), compared to a reconstruction based on the deuterium isotope record of the Dome C ice core (Jouzel et al., 2007; blue). **(c)** Modeled reference deep-ocean temperature anomaly from PI, globally averaged (red), and at 42.5° S (blue), compared to a reconstruction from the Mg/Ca ratio of a sediment core (Elderfield et al., 2012 [E12]; black) drilled at 41° S. **(d)** Modeled reference NH (40–80° N averaged) deep-ocean temperature anomaly from PI (purple), compared to model output from De Boer et al. (2010) ([DB10]; brown) and the modeled reference NH atmospheric temperature anomaly from PI multiplied by a factor 0.2 (cyan).

CPD
10, 2547–2594, 2014

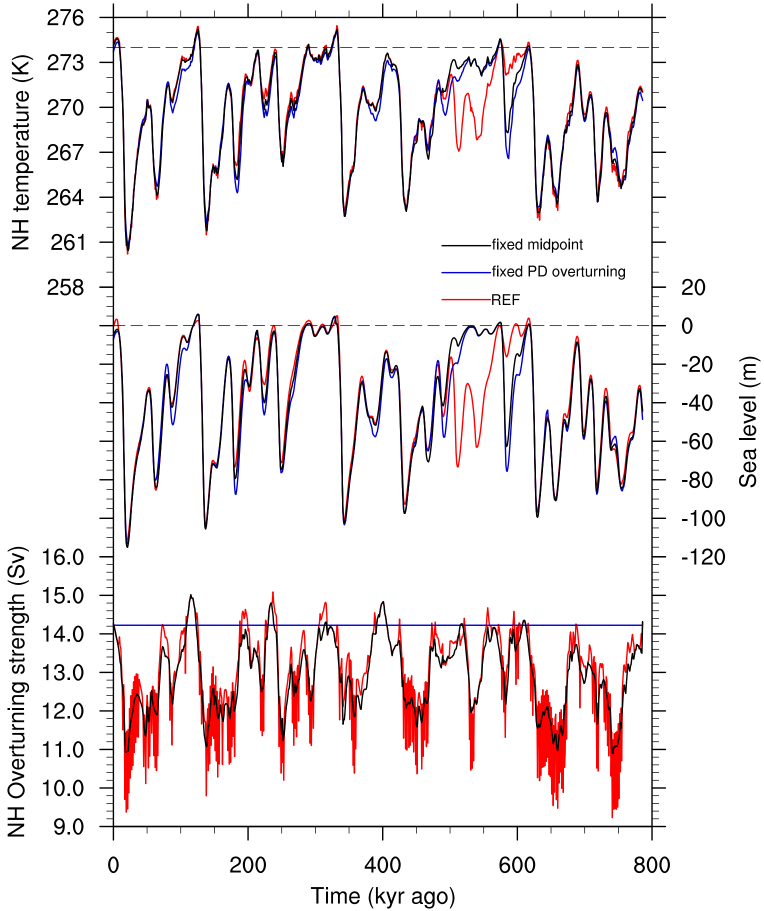

Figure 6. Modeled NH temperature (top), sea level relative to PD (middle), and NH overturning strength (bottom) for the reference run (red), a run with fixed PD overturning (blue) and a run with varying overturning strength, but a fixed midpoint (black).

CPD
10, 2547–2594, 2014

Interaction of ice sheets and climate during the past 800 000 years

L. B. Stap et al.

Title Page
Abstract | Introduction
Conclusions | References
Tables | Figures
◀| |▶
◀ ▶
Back | Close
Full Screen / Esc
Printer-friendly Version
Interactive Discussion

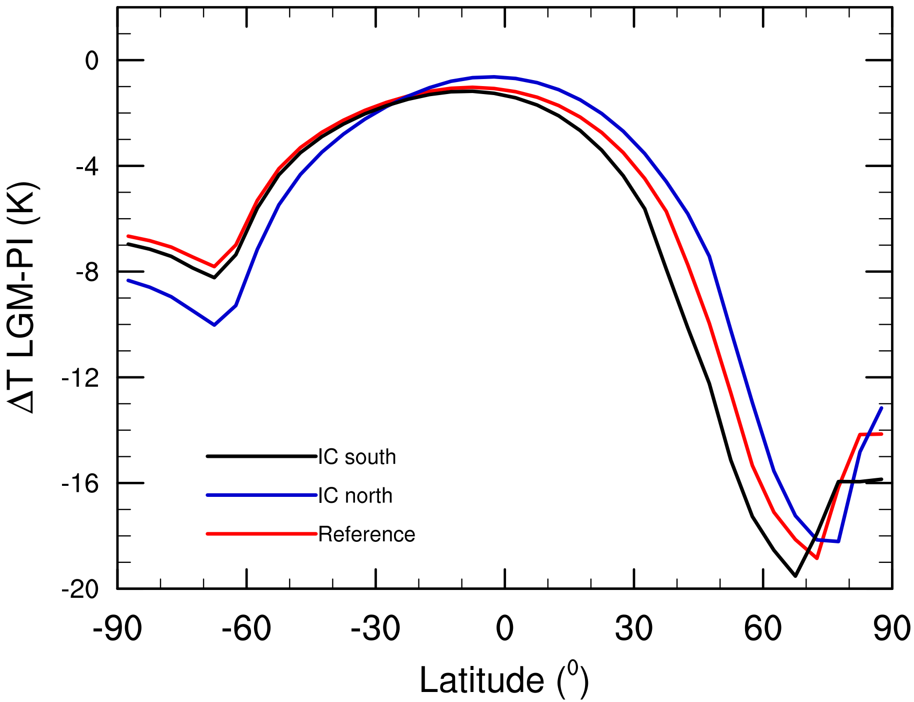

Figure 7. Modeled LGM-PI atmospheric temperature difference, for the reference run (red), a run with the NH ice sheets placed 5° more to the North (blue), and a run with the NH ice sheets placed 5° more to the South (black).

CPD
10, 2547–2594, 2014

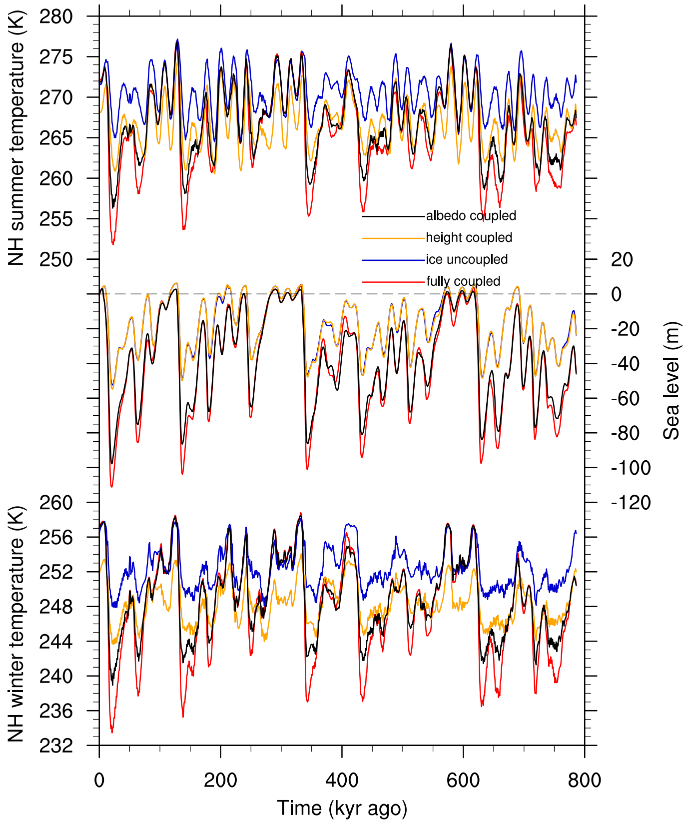

Figure 8. Modeled global temperature (top), sea level realtive to PD (middle), and NH temperature (bottom), for the fully-coupled reference run (red), a run with surface height and albedo in the ZEBCM prescribed as PD values (ice uncoupled; blue), and runs with only surface-height changes (height coupled; orange), and only ice volume (albedo coupled; black) transferred back to the ZEBCM. The missing information on albedo, or surface height, or both, is prescribed as PD values. The temperature data comes from the ZEBCM, the sea level data from the ISM.

CPD
10, 2547–2594, 2014

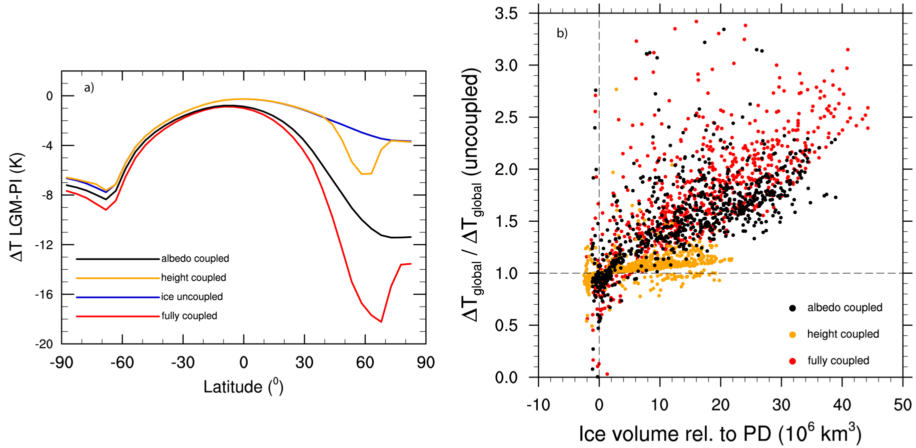

Figure 9. (a) Modeled LGM-PI atmospheric temperature difference, for the same runs as in Fig. 8. **(b)** Ratio of global temperature anomalies from the fully-coupled reference run (red), the height-coupled run (orange) and the albedo-coupled run (black), to those from the ice-uncoupled run, as a function of ice volume in the (partially) coupled run. The temperature data comes from the ZEBCM, the sea level data from the ISM.

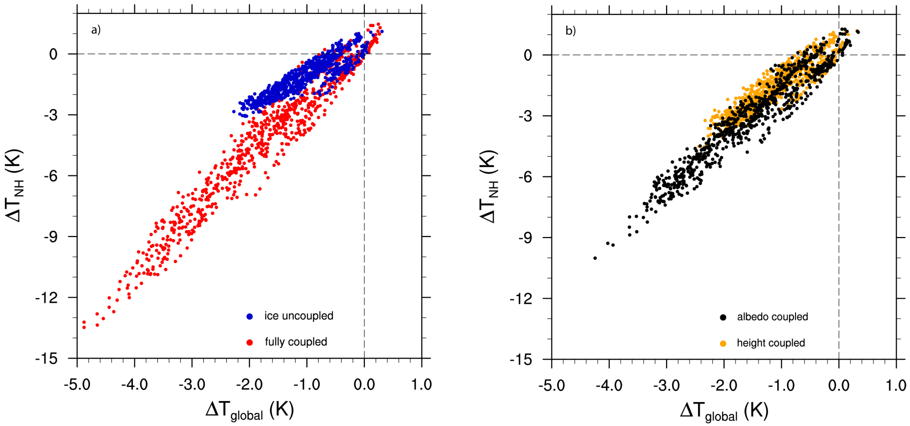

Figure 10. (a) Relation between NH and global temperature anomaly from PI for the fully-coupled reference run (red), and the ice-uncoupled run (blue). **(b)** Relation of NH to global temperature anomaly for the albedo-coupled run (black), and the height-coupled run (orange).

CPD
10, 2547–2594, 2014

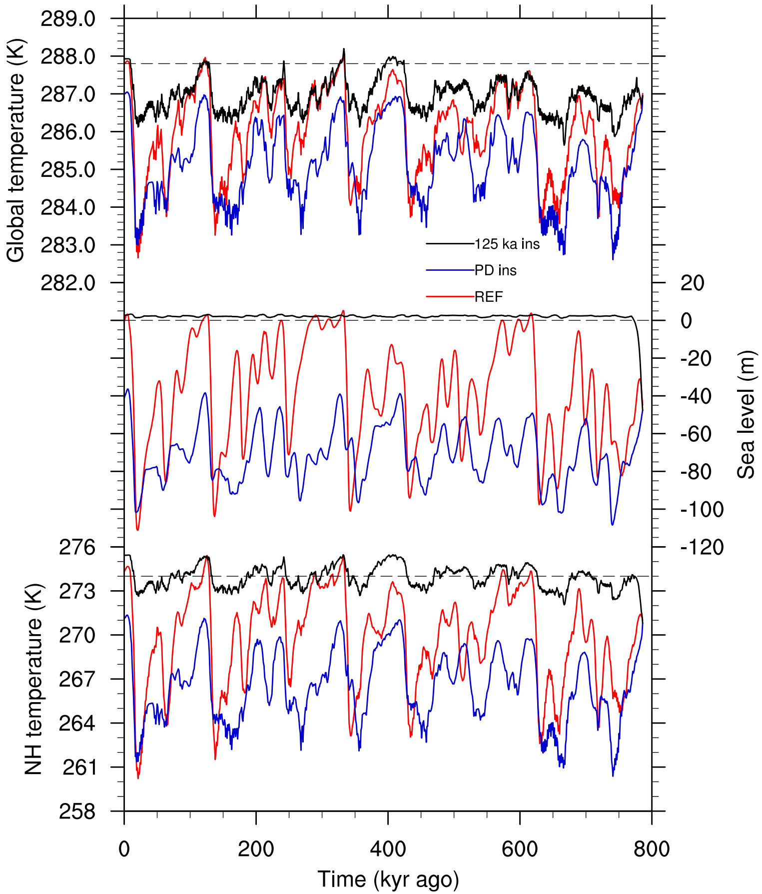

Figure 11. Modeled global temperature (top), sea level relative to PD (middle), and NH temperature (bottom), for the fully-coupled reference run (red), a run with insolation fixed at PD value (blue) and a run with insolation fixed at the precession maximum of 125 kyr ago value (black).

CPD
10, 2547–2594, 2014

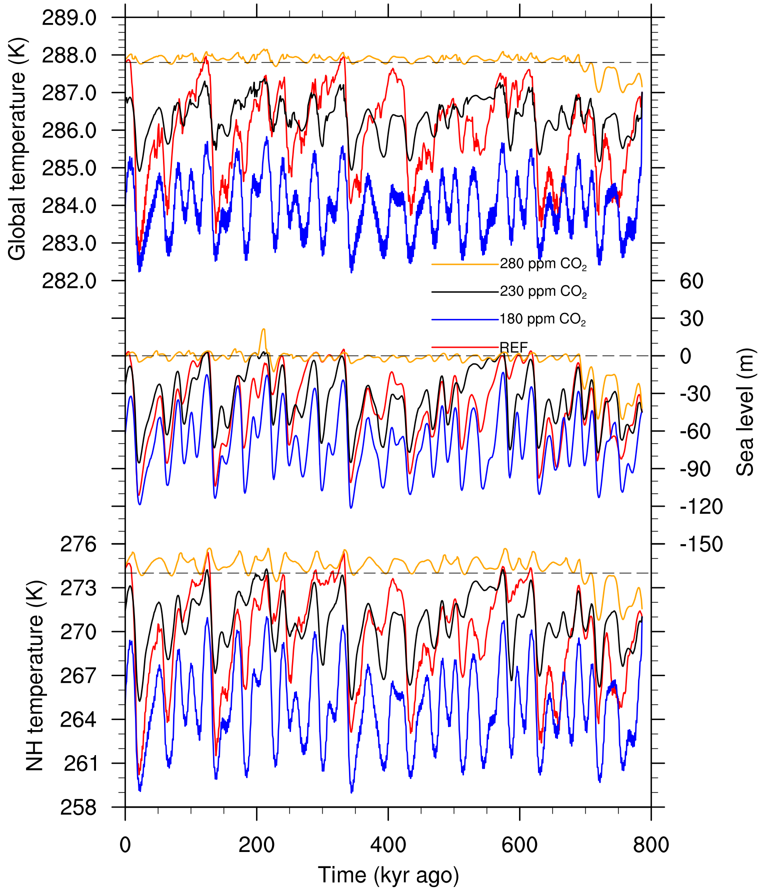

Figure 12. Modeled global temperature (top), sea level relative to PD (middle) and NH temperature (bottom), for the fully-coupled reference run (red), a run with CO_2 fixed at 180 ppm (full glacial value; blue), a run with CO_2 fixed at 230 ppm (intermediate value; black), and CO_2 fixed at 280 ppm (interglacial (PI) value; orange).

CPD
10, 2547–2594, 2014

Interaction of ice sheets and climate during the past 800 000 years

L. B. Stap et al.

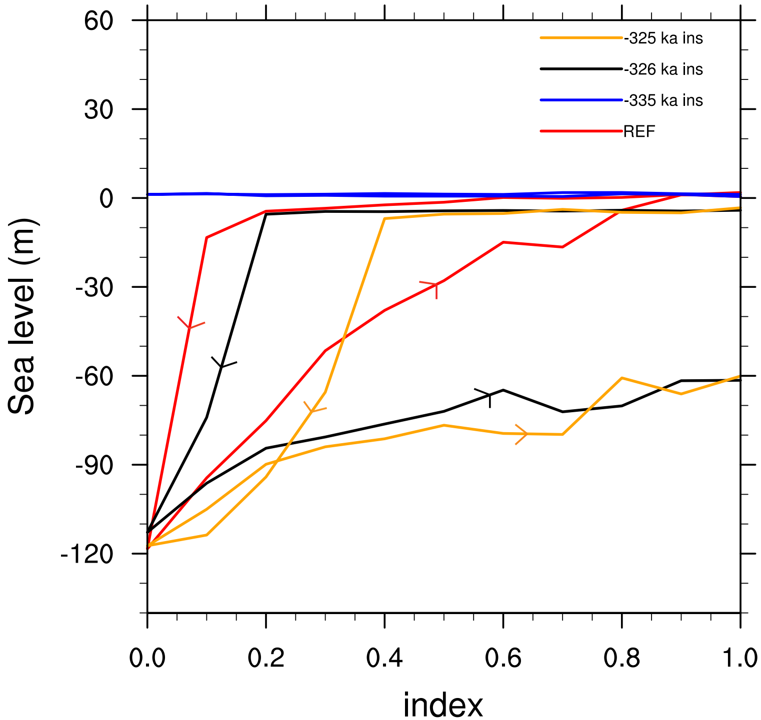

Figure 13. Modeled global sea level in hysteresis tests, where CO_2 is decreased in steps of 10 ppm per 30 kyr from 280 ppm to 180 ppm and then increased in reversed manner. Insolation is kept at constant level of 335 (high NH summer insolation; blue line), 327 (intermediate; black line) and 325 (low; orange line) kyr ago. In the reference case (REF; red line), it is first decreased in steps of 1 kyr from the high to the low extreme, and then increased back to the initial level, in phase with CO_2. An index is assigned to the input values, linearly ranging from favourable (180 ppm CO_2 (and low NH summer insolation for REF); index 0) to unfavourable (280 ppm CO_2 (and high NH summer insolation for REF); index 1) for NH glaciation.

CPD
10, 2547–2594, 2014